Small extracellular vesicles from young adipose-derived stem cells ameliorate age-related changes in the heart of old mice

Jorge Sanz-Ros[1,2], Javier Huete-Acevedo[1], Cristina Mas-Bargues[1], Nekane Romero-García[1,3], Mar Dromant[1], Michel van Weeghel[4,5], Georges E. Janssens[4] and Consuelo Borrás[1]*

Abstract

Background Aging entails a progressive decline in physiological functions, elevating the risk of age-related diseases like heart failure or aortic stenosis. Stem cell therapies, especially those that use paracrine signaling, can potentially mitigate the adverse effects of aging.

Objectives The objective is to explore the potential of small extracellular vesicles (sEVs) derived from young adipose-derived stem cells (ADSC-sEVs) in reversing structural, molecular, and functional changes associated with aging in the heart.

Methods Aged C57BL/6J mice were treated intravenously with ADSC-sEVs from young mice or PBS as controls. Young mice were included to identify specific age-associated changes. The impact of sEV treatment on cardiac function was assessed using transthoracic echocardiography and physical endurance tests. Histological and molecular analyses were conducted on heart tissue to evaluate structural changes and markers of senescence, inflammation, and oxidative stress. A comprehensive metabolomic analysis was also performed on heart tissues to identify changes in metabolic profiles associated with aging and treatment status.

Results The administration of ADSC-sEVs significantly improves several aging-associated cardiac parameters, including oxidative stress, inflammation, and cellular senescence reductions. We also report on the age-related reversal of myocardial structure and function changes, highlighted by decreased fibrosis and improved vascularization. Notably, echocardiographic assessments reveal that sEV treatments ameliorate diastolic dysfunction and left ventricle structural alterations typically associated with aging. Furthermore, the treatment shifts the heart metabolome towards a more youthful profile.

Conclusions These results denote the potential of ADSC-sEVs as a novel, noninvasive therapeutic strategy for mitigating cardiac aging-associated functional decline.

Keywords Aging, Heart failure, Regenerative medicine, Extracellular vesicles, Inflammation, Metabolomics

*Correspondence:
Consuelo Borrás
consuelo.borras@uv.es

Full list of author information is available at the end of the article

Background

Aging is accompanied by a decline in tissue regenerative capacity, increasing susceptibility to various age-related diseases. While stem cell therapies have shown promise in regenerative medicine, recent studies indicate that their therapeutic effects are primarily mediated by paracrine mechanisms rather than direct tissue integration. Extracellular vesicles (EVs), including small extracellular vesicles (sEVs), have emerged as crucial mediators of intercellular communication, carrying a diverse range of proteins, nucleic acids, and lipids. Traditionally, EVs were classified based on their biogenesis pathways, with microsvesicles budding directly from the plasmatic membrane, and exosomes being formed through the endosomal pathway and contained in multivesicular bodies [1]. While these differences in origin exist, EVs are now broadly categorized based on their size as current isolation methods usually rely on vesicle size to separate vesicle populations. Large extracellular vesicles (lEVs) range from approximately 200 nm to 1 μm in diameter and sEVs typically range from 30 to 200 nm [2].

Mesenchymal stem cells (MSCs) have been extensively investigated for their regenerative potential due to their ease of isolation, culture, and low immunogenicity. However, the use of MSCs is complicated by their limited survival and integration into host tissues. In contrast, the secretome of MSCs, particularly EVs, offers advantages such as stability, ease of dosage, and lower immunogenicity, with several ongoing clinical trials for various conditions. EVs are also being studied as regulators of aging-related processes, participating in cellular senescence, oxidative stress, telomere dysfunction, inflammation, and metabolic dysregulation.

The average human lifespan is increasing, leading to a significant rise in the population aged 65 and older, a trend expected to continue over the next two decades. Within this demographic, cardiovascular disease remains the primary cause of mortality, coupled with rising treatment costs. Aging, an inherent aspect of life, is the predominant risk factor for cardiovascular diseases. Therefore, the relationship between cardiovascular disease and the molecular and cellular aspects of aging is evident. Heart tissue undergoes several age-associated changes, such as fibrosis, valvular degeneration, calcification, cardiomyocyte hypertrophy, degeneration of the conduction system, and cellular senescence-related alterations. These changes contribute to the development of several age-related diseases, whose prevalence and incidence are increasing, such as heart failure with preserved ejection fraction (HFpEF) and aortic stenosis.

The present study focuses on the therapeutic potential of ADSC-sEVs in mitigating age-related changes in the heart. We demonstrate that ADSC-sEVs exert anti-aging effects in the heart of old mice by modulating cellular senescence, oxidative stress, inflammation, and metabolism.

Materials and methods

Mouse model

This investigation adhered rigorously to all relevant federal and institutional guidelines. The University of Valencia Animal Ethics Committee, following European Union (EU) regulations on animal research, approved the protocol under identification number A1508582840889 ("Efecto de la administración de vesículas extracelulares de células madre de tejido adiposo derivadas de ratones jóvenes en ratones envejecidos", approved on 31-01-2018). Mice were housed in the animal center of the Central Unit for Research in Medicine (UCIM) of the Faculty of Medicine and Odontology of the University of Valencia. Animals were kept in the facility at $22 \pm 2\,°C$, with a relative humidity of 60% under 12–12 h of dark-light cycles and with access to food and water *ad libitum*. The mice in the study were of a C57BL/6J background, randomly selected to treatment with EVs or with PBS as a control. Mouse ages for the present study were chosen based on recommendations from the American Federation of Aging Research (Principles of Animal Use for Gerontological Research). The average age of the mice that received sEVs was 21.925 months, while those that received PBS had an average age of 21.975 months. Both genders were included, and, when possible, littermates of the same sex were used in different groups. The sample size was determined using G*Power, and random assignment to experimental groups was conducted. Each mouse received two doses separated by 7 days, comprising either 20 μg of sEV protein or PBS as a control. The doses were administered intravenously to mice via the tail vein in a total volume of 100 μl diluted in PBS. The protocol was replicated across several batches of old mice treated with sEVs versus PBS as a control. Mouse weight was annotated during the experimental procedure as a surrogate marker of toxicity. Upon euthanasia by cervical dislocation 30 days post-treatment with sEVs/PBS, the heart was collected, weighed, and stored at -80 °C for further processing. Please see the Major Resources Table in the Supplemental Materials. The work has been reported in line with the ARRIVE guidelines 2.0.

Stem cell isolation and culture

Stem cell culture involved obtaining mesenchymal stem cells (MSCs) from inguinal fat pads of mice aged 3 to 6 months (ADSCs) according to a previously described protocol [3]. In brief, inguinal fat pads were extracted under sterile conditions, and adipose tissue was subjected to collagenase I digestion (0.1% type I collagenase and 1% BSA in PBS supplemented with 2 mM CaCl2). The digested tissue was centrifuged twice at 300 g to remove

floating adipocytes, and the stromal vascular fraction was seeded. Some endothelial cells were observed in passage 0 but were lost after passage 1. Cells in passages 2 or 3 were used, cultured in high-glucose Dulbecco's modified Eagle's medium (DMEM) with 10% FBS and 1% penicillin/streptomycin. Culture conditions included 37 °C, 5% CO2, and 3% O2.

ADSCs' characterization

As referenced in our previous work, ADSCs' characterization was conducted using flow cytometry [4]. We assessed the presence of MSC markers CD29 and CD44, using CD45 and CD31 as negative controls to identify potential contaminants in the culture. Once the cells reached 80% confluency, they were trypsinized and resuspended in fluorescence-activated cell sorting (FACS) buffer that contained 10% FBS and 1% sodium azide in PBS. For each condition, 100,000 cells were stained with antibodies at 1 μg/μl and incubated for 30 min at 4 °C. The antibodies used, all obtained from BioLegend, were as follows: CD29 R-phycoerythrin/Cyanine7 (PE/Cy7), catalog number 10,222; CD31 PE, catalog number 102,507; CD44 Alexa Fluor 488, catalog number 103,015; and CD45 PE, catalog number 103,106.

Isolation of ADSC-derived sEVs

The isolation of ADSC-derived small extracellular vesicles (sEVs) involved culturing ADSCs in high-glucose DMEM supplemented with 2% exosome-depleted FBS and 1% penicillin/streptomycin (Gibco, A2720803) for 48 h. The conditioned medium was then collected, and sEVs were isolated through differential ultracentrifugation. The culture medium was centrifuged at 2000 g for 10 min and centrifuged at 20,000 g for 30 min to remove whole cells, cell debris, and larger extracellular vesicles (EVs). The resulting supernatant was subjected to ultracentrifugation at 100,000 g for 70 min. The pelleted vesicles were re-suspended in PBS and underwent another round of ultracentrifugation at 100,000 g for 70 min for thorough washing, followed by re-suspension in PBS. sEVs isolated from the conditioned medium were stored at 4 °C and used for treatment within 24 h. The dosage of sEVs was determined by protein quantification using the Lowry method.

Transmission electron microscopy and Immunogold labeling of sEVs

The isolated sEVs were fixed in a 2% paraformaldehyde (PFA) solution in 0.1 M PBS for 30 min. A glow discharge technique (30 s, 7.2 V) using a Bal-Tec MED 020 Coating System was applied to carbon-coated copper grids. Subsequently, these treated grids were placed over the sample drops for 15 min. The grids with attached sEVs were then immersed in a 0.1 M PBS solution for washing,

followed by an additional fixation step in 1% glutaraldehyde for 5 min. After thorough washing in distilled water, the grids were contrasted with 1% uranyl acetate and embedded in methylcellulose. Excess fluid was carefully removed, and the samples were allowed to dry before examination using a transmission electron microscope, FEI Tecnai G2 Spirit (Thermo Fisher Scientific, OR, USA). Image acquisition was performed using a digital camera, Morada (EMSIS GmbH, Münster, Germany). For immunogold labeling, 8 μl of isolated sEVs were fixed in 2% PFA in 0.1 M PBS for 30 min. Carbon-coated nickel grids were then positioned over these sEV drops for 15 min. After washing in 0.1 M PBS, the grids were blocked in a solution of 0.1 M glycine and 0.3% BSA for 10 min. The grids were subsequently incubated with the primary antibody anti-CD63 (MBL, D263-3) at a dilution 1:100 for 1 h. Following another blocking step for 10 min, the grids were exposed to Gold 6 nm–conjugated goat anti-rat secondary antibody (Abcam, ab105300) at a dilution of 1:1000 for 1 h. Lastly, a standard negative staining procedure was applied after thorough washing, and the samples were observed under a transmission electron microscope, as previously described.

PKH26 staining

For in vivo tracking of sEVs, we obtained sEVs from the conditioned medium of young ADSCs. Subsequently, these sEVs were labeled with 5 μM PKH26 (Sigma-Aldrich, MINI26-1KT) following the first ultracentrifugation. Following the labeling, the sEVs were resuspended in PBS and subjected to an additional round of washing through ultracentrifugation. A total of 20 μg of PKH26-labeled sEVs in 100 μL of PBS were injected into aged mice (20 months), and control mice were injected with 100 μL of a PBS solution containing 5 μM PKH26. The mice were euthanized 24 h later, and heart tissue was harvested, fixed in 4% PFA for 24 h, and cryoprotected in 30% sucrose for another 24 h. Ten-micrometer cryostat slices were mounted on slides. Sections were blocked with 10% normal goat serum (Invitrogen) in PBS containing 0.05% Tween 20 (PBS-t) and incubated overnight at 4 °C with a primary antibody against Desmin (Cell Signaling, 5332; 1:500 dilution) and with Alexa Fluor 488 anti-rabbit (Abcam, ab150077; 1:2000 dilution) for 2 h at room temperature as the secondary antibody. Sections were counterstained with DAPI (Invitrogen) at a 1:1000 dilution for 30 min at room temperature and then mounted on coverslips using an aqueous mounting medium sealed with nail polish. Imaging was performed using an Olympus FV1000 confocal laser scanning biological microscope. Images were processed in ImageJ while maintaining equal ratios.

Echocardiography assessment in mice

Anesthesia was induced in a chamber with 2–3% isoflurane delivered in a mixture of oxygen (1–2 L/min). Once anesthetized, mice were transferred to a nose cone for continuous isoflurane inhalation at a 1–2% maintenance concentration. Anesthesia depth was monitored throughout the procedure by assessing the respiratory rate and pedal withdrawal reflex. Echocardiography was performed using an imaging system (GE Versana Active Veterinary Ultrasound Scanner) equipped with a 12-MHz transducer for small animals. Mice were positioned in a supine position with external heating to maintain body temperature. The chest area was shaved, and ultrasound gel was applied for optimal acoustic coupling. Two-dimensional (2D) M-mode and pulsed Doppler images were acquired in various views, including parasternal long-axis, short-axis, and apical views. For data analysis, images were analyzed using the same ultrasound scanner for acquisition. Standard echocardiographic parameters shown in the results section were measured for fractional shortening (FS) calculation, M-mode images were used to measure left ventricle end-diastolic diameter (LVEDD), and end-systolic diameter (LVESD), FS = LVEDD– LVESD / LVEDD x 100.

Treadmill physical endurance test

The animals underwent a progressive intensity treadmill test (Treadmill Control LE 8710 Panlab, Harvard Apparatus) to assess their endurance, measured by maximum time running. Following a warm-up period, the treadmill belt velocity was incrementally elevated until the animals reached exhaustion, indicating their inability to continue running. The test commenced with an initial 4-minute session at 10 cm/s, followed by successive increments of 4 cm/s every 2 min. Exhaustion was defined as the point at which a mouse remained on the shock grid for 5 s instead of actively running.

Histology

Heart tissue was freshly frozen in liquid nitrogen and 10-micron slices were obtained using a cryostat for histological staining and immunofluorescence. Hematoxylin and eosin staining (Sigma-Aldrich, MHS32, and E4009, respectively) or Sirius red staining (Sigma-Aldrich, 365548) was performed on the sections, followed by mounting and sealing for morphometric analysis. Images were captured using an optical microscope (Leica), and three images from different areas of each slice were obtained. Morphometric analysis of heart sections was conducted using ImageJ.

Immunofluorescence imaging

Ten-micrometer tissue slices were mounted on slides and fixed with ice-cold acetone for 20 min. For permeabilization, slices were incubated in 1% Triton X-100 in PBS for 10 min. Sections were blocked with 10% normal goat serum (Invitrogen) in PBS with 0.05% Tween 20 (PBS-t) and incubated with primary antibodies overnight at 4 °C in the same buffer. After primary antibody incubation, sections underwent three 10-minute PBS-t washes and were then incubated with secondary antibodies for 2 h at room temperature. Subsequent washes were performed, and tissues were counterstained with DAPI (Invitrogen; 1:1000 dilution) for 30 min at room temperature. Coverslips were mounted with an aqueous mounting medium and sealed with nail polish. Images were acquired using an Olympus FV1000 confocal laser scanning biological microscope. Image processing was carried out using CellProfiler with custom pipelines for automatic cell counting and analysis of CD3, LMNB1, and γH2AX positive cells. CD31 area was calculated using ImageJ, with uniform adjustments to levels. Three images from different areas of each slice were obtained.

The following antibodies and concentrations were used:

CD31 staining: Alexa Fluor 647 anti-mouse CD31 antibody (Biolegend, 102515, 1:50 dilution).

LMNB1 staining: anti-LMNB1 (Proteintech, 12987-1-AP; 1:50 dilution) and Alexa Fluor 488 anti-rabbit (Abcam, ab150077; 1:2000 dilution); a minimum of 150 nuclei were analyzed per sample.

γH2AX staining: anti-γH2AX (Cell Signaling Technology, 9718 S; 1:1000 dilution) and Alexa Fluor 488 anti-rabbit (Abcam, ab150077; 1:2000 dilution); a minimum of 150 were analyzed per sample.

CD3 staining: anti-CD3 (Proteintech, 17617-1-AP; 1:1000 dilution) and Alexa Fluor 647 anti-rabbit (Abcam, ab150079, 1:2000 dilution).

Quantification of lipid peroxidation by HPLC

Heart tissue was lysed using a KPi-EDTA buffer [50 mM KPi and 1 mM EDTA (pH 7.4)], and the levels of lipid peroxidation were assessed by quantifying malondialdehyde (MDA) using high-performance liquid chromatography (HPLC). MDA was determined as an MDA–thiobarbituric acid (TBA) adduct following a previously established method. This approach relies on the hydrolysis of lipoperoxides and the subsequent formation of a TBA-MDA2 adduct, which was detected using reverse-phase HPLC and quantified at 532 nm. The chromatographic technique was carried out under isocratic conditions, with the mobile phase comprising a mixture of monopotassium phosphate at 50 mM (pH 6.8) and acetonitrile (70:30). The MDA levels in each sample were normalized to the protein concentration determined by the Lowry method.

Protein oxidation quantification with Immunoblotting

Total protein carbonylation was detected by immunoblotting using the OxyBlot Protein Oxidation Detection kit (Merck) following the manufacturer's instructions. In brief, tissues were lysed in tris/SDS/glycerol buffer, and protein concentration was determined using the Lowry method. Subsequently, 20 μg of proteins were separated on SDS polyacrylamide gels and transferred onto nitrocellulose membranes. The membranes were blocked with 3% BSA in PBS-t for 60 min at room temperature and then incubated overnight at 4 ℃ with the primary antibody from the kit. After three washes (10 min each) with PBS-t, the membranes were incubated with the secondary antibody for 120 min at room temperature. Following three additional washes with PBS-t, the membranes were developed with Luminol (Sigma-Aldrich) using the ImageQuant LAS4000 system. Image analysis was performed in ImageJ, and Ponceau staining of the membranes served as the loading control.

Interleukin quantification

We utilized two commercially available enzyme-linked immunosorbent assay (ELISA) kits for the quantitative analysis of IL-6 (Abcam, ab100713) and IL-8 (Abcam, ab234567), adhering to the manufacturer's provided instructions. In brief, tissues underwent lysis using specific buffers included in each kit, protein concentration was determined using the Lowry method, and samples were appropriately diluted at ratios of 1:5. Absorbance at 450 nm was quantified using the Molecular Devices SPECTRAmax Plus 384. All samples were subjected to duplicate assays.

Metabolomics

Metabolomics was performed as previously described, with minor adjustments [5, 6]. A 75 μL mixture of the following internal standards in water was added to approximately 3 mg of freeze-dried heart tissue: adenosine-$^{15}N_5$-monophosphate (100 μM), adenosine-$^{15}N_5$-triphosphate (1 mM), D_4-alanine (100 μM), D_7-arginine (100 μM), D_3-aspartic acid (100 μM), D_3-carnitine (100 μM), D_4-citric acid (100 μM), $^{13}C_1$-citrulline (100 μM), $^{13}C_6$-fructose-1,6-diphosphate (100 μM), guanosine-15N_5-monophosphate (100 μM), guanosine-$^{15}N_5$-triphosphate (1 mM), $^{13}C_6$-glucose (1 mM), $^{13}C_6$-glucose-6-phosphate (100 μM), D_3-glutamic acid (100 μM), D_5-glutamine (100 μM), $^{13}C_6$-isoleucine (100 μM), D_3-leucine (100 μM), D_4-lysine (100 μM), D_3-methionine (100 μM), D_6-ornithine (100 μM), D_5-phenylalanine (100 μM), D_7-proline (100 μM), $^{13}C_3$-pyruvate (100 μM), D_3-serine (100 μM), D_5-tryptophan (100 μM), D_4-tyrosine (100 μM), D_8-valine (100 μM). Subsequently, 425 μL water, 500 μL methanol, and 1 mL chloroform were added to the same 2 mL tube before thorough mixing and centrifugation for 10 min at 14.000 rpm. The top layer, containing the polar phase, was transferred to a new 1.5 mL tube and dried using a vacuum concentrator at 60 ℃. Dried samples were reconstituted in 100 μL methanol/water (6/4; v/v). Metabolites were analyzed using a Waters Acquity ultra-high-performance liquid chromatography system coupled to a Bruker Impact II™ Ultra-High Resolution Qq-Time-Of-Flight mass spectrometer. Samples were kept at 12 ℃ during analysis and 5 μL of each sample was injected. Chromatographic separation was achieved using a Merck Millipore SeQuant ZIC-cHILIC column (PEEK 100 × 2.1 mm, 3 μm particle size). Column temperature was held at 30 ℃. The mobile phase consisted of (A) 1:9 acetonitrile: water and (B) 9:1 acetonitrile: water, both containing 5 mM ammonium acetate. Using a flow rate of 0.25 mL/min, the LC gradient consisted of: Dwell at 100% Solvent B, 0–2 min; Ramp to 54% Solvent B at 13.5 min; Ramp to 0% Solvent B at 13.51 min; Dwell at 0% Solvent B, 13.51–19 min; Ramp to 100% B at 19.01 min; Dwell at 100% Solvent B, 19.01–19.5 min. Equilibrate the column using a 0.4 mL/min flow at 100% B from 19.5 to 21 min. MS data were acquired using negative and positive ionization in full scan mode over the range of m/z 50-1200. Data were analysed using Bruker TASQ software version 2021b (2021.1.2.452). All reported metabolite intensities were normalized to dry tissue weight, as well as to internal standards with comparable retention times and response in the MS. Metabolite identification was based on a combination of accurate mass, (relative) retention times, and fragmentation spectra, compared with the analysis of a library of standards. Statistical analysis and visualization of the acquired data were done in an R environment using the ggplot2, ropls, and mixOmics packages [7, 8].

Statistical analysis

Ratios depicting the comparison of physical test values after treatment against baseline were calculated and presented as percentages over baseline, with the baseline defined as 0%. Outliers were assessed in all groups using the ROUT method (Q = 2%), with no exclusion of any data point. The normality of each group was assessed using the Shapiro-Wilk test. For pairwise comparisons, either the Unpaired Student's t-test or the Mann-Whitney test was employed, depending on the data distribution. In the case of multiple comparisons, ANOVA was applied, with Tukey's multiple comparisons serving as a post hoc test. Alternatively, for nonparametric data, the Kruskal-Wallis test was utilized, with Dunn's multiple comparisons as the post hoc test. Each data point presented in the manuscript represents a biological replicate. GraphPad Prism 9.0 software was utilized for both analysis and graphical design if not otherwise stated.

Results

Intravenously delivered sEVs from young ADSCs effectively reach the heart of old mice

Firstly, we conducted a characterization of the vesicles isolated from the cell culture supernatants of young ADSCs (Fig. 1A-B), according to the minimal information for studies of extracellular vesicles (MISEV) recommendations for the characterization and functional studies of sEVs [2]. We utilized transmission electron microscopy (TEM) to evaluate the size and morphology of the isolated vesicles, revealing round-shaped vesicles ranging from 50 to 200 nm in diameter (Fig. 1C). Additionally, the presence of CD63, a classical marker of sEVs, in the vesicle membrane was corroborated through immunogold labeling (Fig. 1C). sEVs are delivered to several tissues after intravenous injection, with a preference for the liver [9]. To demonstrate the delivery and uptake of sEVs in the heart tissue, we labeled the sEVs with a lipophilic dye (PKH26) and administered them into the bloodstream of old mice through tail vein injection. Subsequent histological study with fluorescence microscopy of the heart tissue revealed the dye uptake in this organ, colocalizing with cardiomyocyte fibers (Fig. 1D).

ADSC-sEVs improve functional parameters associated with aging in the heart of old mice

We then assessed the impact of ADSC-sEVs on functional parameters associated with cardiac aging in old mice. To this end, we performed transthoracic echocardiography with a transducer designed for small animals in young (3–6 months) and old C57BL/6J mice (20–24 months), to obtain which parameters are altered with age in this mouse strain. To better characterize the effect of sEVs on echocardiographic parameters in old mice, we performed echocardiography before treatment (Day 0) and 30 days after treatment (Day 30) with PBS or sEVs (Fig. 2A).

Heart rate exhibited no significant changes from young to old mice, and this pattern persisted in old mice following sEVs treatment (Fig. 2B-C). Fractional shortening remained unaltered across age groups and treatment status, indicating little changes in systolic function during mouse aging, in line with previous studies [10] (Fig. 2D-E). Peak aortic velocity tended to increase in old mice, probably suggesting a propensity to develop aortic valve calcification in these mice, as previously noted [10, 11]. sEVs treatment didn't significantly reduce this trend (Fig. 2F-G).

The most prominent functional changes associated with aging in the heart, both in mice and humans, are the increased left ventricle (LV) mass and reduced diastolic function [12, 13]. Indeed, we found that LV posterior wall thickness exhibited an age-related increase in old mice compared to the young group; however, treatment

with sEVs reversed this trend, reducing wall thickness (Fig. 2H-I). Regarding the pulsed Doppler of the LV filling, peak E wave velocity increased with age in mice; conversely, peak A wave velocity decreased with age, leading to an increased E/A relationship (> 2) in the old mice. This indicates an altered diastolic function with a restrictive pattern, where LV filling depends mainly on the proto-diastolic wave. Treatment with sEVs in old mice partially reversed this pattern, with a significant reduction of the peak E wave velocity and a non-significant trend showing reduced E/A ratios (Fig. 2J-O).

To assess overall physical endurance and potential indirect effects on cardiac function, we conducted a treadmill test 30 days after treatment (Day 30) with PBS or sEVs. Although treadmill performance isn't specific to cardiac function, it offers a comprehensive evaluation of multiple systems, including the cardiovascular, respiratory, and musculoskeletal systems. Young mice showed higher performance levels in the treadmill test than old mice (Fig. 2P). When splitting by sex, female mice treated with sEVs showed an increased endurance in this test compared to old female control mice (Fig. 2Q), which was not significant in male mice (Fig. 2R). This indicates a sex-dependent effect of the treatment on this parameter, which we did not observe in other measurements, a finding commonly seen in various anti-aging interventions [14, 15].

Collectively, these findings show the potential of ADSC-sEVs in ameliorating age-associated alterations in cardiac functional parameters.

ADSCs-sEVs alleviate age-related histological alterations of the mouse heart

To further correlate the effect of sEVs on functional parameters, we explored structural alterations in heart tissue at the histological level. Some of these changes include an increase in LV mass, myocardial fibrosis, and altered vascularization, all of which contribute to functional decline, especially the diastolic dysfunction observed during aging [11, 16, 17].

First, we measured the heart weight normalized by the mice's total body weight (TBW) as an indicator of total heart mass. Old mice treated with sEVs showed a lower heart weight ratio when compared to controls (Fig. 3A), indicating a lower heart mass; the comparison between young and old mice was non-significant, probably because TBW is much lower in young mice. Histological analysis with Sirius red staining demonstrated an increase of fibrotic tissue in the hearts of old mice compared to young ones. Treatment with ADSCs-sEVs significantly decreased fibrotic tissue (Fig. 3B and D), suggesting a protective effect against aging-associated cardiac remodeling and fibrosis. Furthermore, assessment of vascularization through CD31 immunostaining
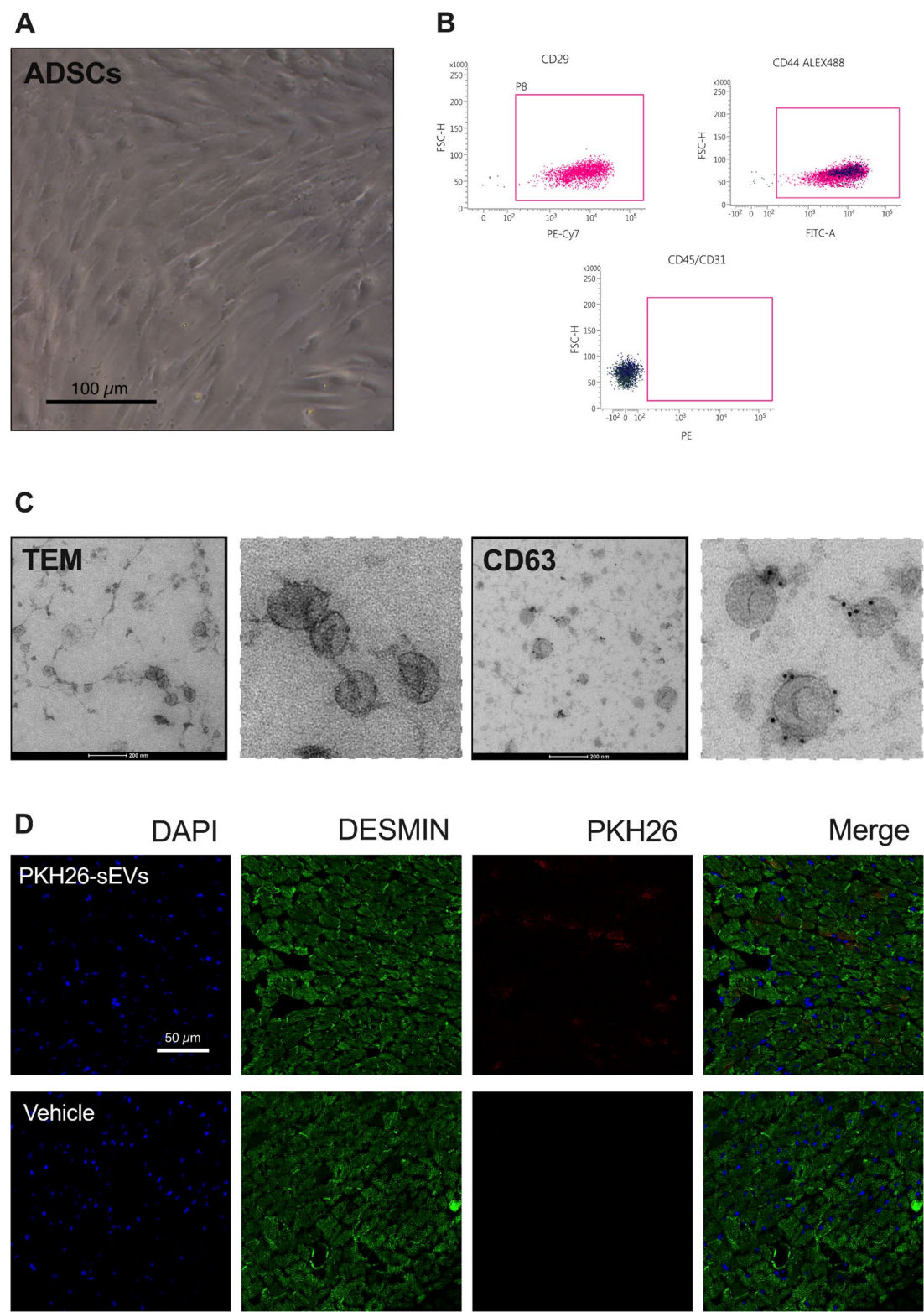
Fig. 1 Systemically delivered ADSC-sEVs reach the heart of old mice. (**A**) Representative image of passage 2 ADSCs in culture. (**B**) Flow cytometry characterization of ADSCs shows MSC markers (CD29 and CD44) and negative controls (CD31 and CD45). (**C**) Representative transmission electron microscopy images of ADSC-sEVs and immuno-gold labeling of the CD63 protein in sEVs samples. (**D**) Representative images of heart tissue from old mice treated with either PKH26 labeled ADSC-sEVs or vehicle as controls and stained with Desmin
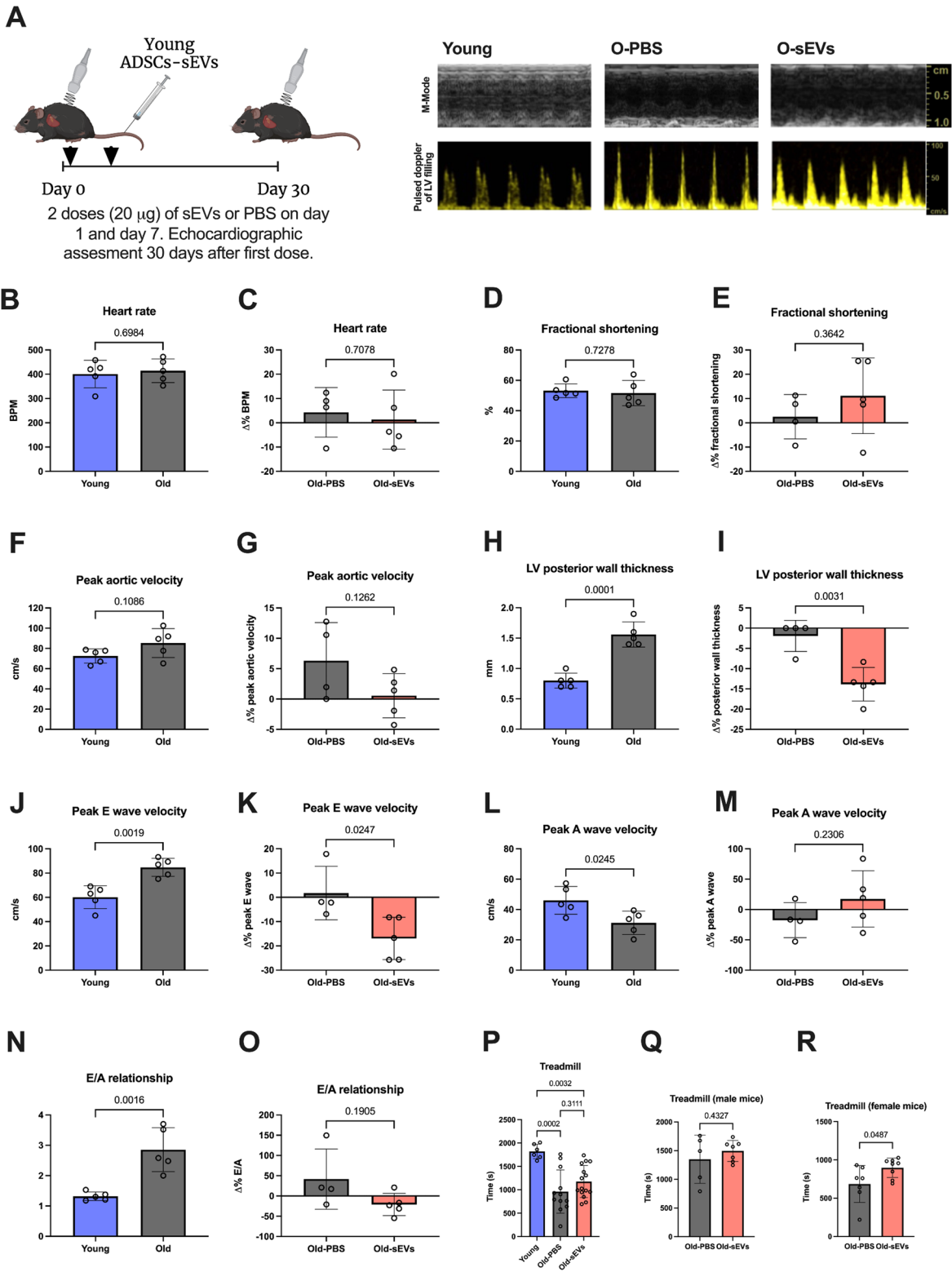
Fig. 2 (See legend on next page.)

(See figure on previous page.)

Fig. 2 Effect of ADSC-sEVs on echocardiographic and functional parameters of old mice. (**A**) Schematic representation of the experimental design and representative images of M-mode and pulsed Doppler from transthoracic echocardiography. (**B-C**) Quantification of the heart rate. (**D-E**) Quantification of the fractional shortening as measured from LVEDD and LVESD measurements. (**F-G**) Quantification of peak aortic velocity from pulsed Doppler. (**H-I**) Quantification of LV posterior wall thickness. (**J-K**) Quantification of peak E wave velocity from pulsed Doppler of LV filling. (**L-M**) Quantification of peak A wave velocity from pulsed Doppler of LV filling. (**N-O**) E/A wave ratio measurement. (**P-R**) Quantification of maximum time running in the treadmill test, computed values and separated by sex. For young vs. old comparisons, absolute values are shown. For O-PBS vs. O-sEVs echocardiography comparisons, data are shown as the change in percentage from the baseline before treatment with sEVs/PBS. All data are shown as means ± SD. B-O: $n = 5$ per group. P: $n = 6$ for young, 12 for Old-PBS, 15 for Old-sEVs. Q: $n = 5$ for Old-PBS, 7 for Old-sEVs. R: $n = 7$ for Old-PBS, 8 for Old-sEVs

unveiled a significant reduction of the CD31 + area in the aged heart. At the same time, we observed an increase in the CD31 + area in heart slices from mice treated with ADSC-sEVs (Fig. 3C and E), indicating a pro-angiogenic effect of sEVs. This EV-dependent enhancement in vascularization has also been observed previously in several tissue damage models [18, 19].

These results show the role of ADSC-sEVs in counteracting age-related cardiac structural changes in aged mice.

Cellular and molecular markers of aging are partially reversed by young ADSCs-sEVs in the heart of old mice

Some of the molecular and cellular markers of aging are common to the different species and tissues, such as oxidative damage, pro-inflammatory factors accumulation, and cellular senescence [20]. Here, we investigated the impact of young ADSCs-sEVs on these markers in heart tissue. Oxidative damage is commonly viewed as a contributor to the aging process, and the heart is particularly sensitive to oxidative damage [21]. We measured MDA as a marker of lipid peroxidation [22] and protein carbonylation as a marker of protein oxidation [23], heart tissue of old mice exhibited higher levels of lipid peroxidation and protein carbonylation when compared to their young counterparts, indicative of increased oxidative damage in the aged heart (Fig. 4A-B). Remarkably, treatment with sEVs reduced these markers, suggesting a mitigating effect on oxidative stress-induced damage (Fig. 4A-B).

Regarding the pro-inflammatory landscape that usually accompanies aging [24], we measured the levels of two factors that are usually increased in aged tissues, interleukin-6 (IL-6) and interleukin-8 (IL-8), pro-inflammatory cytokines that are also tightly associated with the senescence-associated secretory phenotype (SASP) [25] and have been proposed as mediators of age-related changes in cardiac tissue, including hypertrophy [26, 27]. Both factors displayed an age-related increase in the heart, notably attenuated following sEVs treatment (Fig. 4C-D). As another tissue inflammatory, we measured the infiltration of T cells (CD3+) outside of the blood vessels in the heart tissue using immunofluorescence, which was almost non-existent in the young tissues and followed a similar increasing age-related pattern. Again, treatment with sEVs partially reversed this trend (Fig. 4E-F).

We then measured two closely related markers of cellular senescence and DNA damage. We employed Lamin B1 (LMNB1) immunofluorescence to quantify cellular senescence; the loss of LMNB1 is widely used in tissues to measure the levels of senescent cells [28]. We found a reduced proportion of LMNB1 + cells in the heart with aging, while the treatment with ADSCs-sEVs showed a non-significant increase in this marker (Fig. 4G-H). The γH2AX marker of DNA damage exhibited an age-related increase in the heart, along with the results regarding oxidative damage to proteins and lipids; the treatment with ADSCs-sEVs reduced the levels of this marker (Fig. 4I-J).

These findings suggest that treatment with young ADSCs-sEVs ameliorates cellular and molecular markers associated with aging in the heart, reducing oxidative and DNA damage and counteracting the age-related pro-inflammatory environment.

Treatment with ADSC-sEVs switches the heart metabolome of old mice to a youthful state

Although a significant body of evidence shows that impaired metabolism in the heart accompanies the aging process and contributes to different age-associated alterations [29–31], little is known about specific changes in different metabolites with age and with targeted aging interventions. We conducted a comprehensive metabolomic analysis of the heart to substantiate further our findings on the beneficial effects of ADSC-sEVs on aged heart tissue. This allowed us to explore the alterations in the metabolic landscape of the heart that accompany aging and investigate how ADSC-sEV treatment influences these changes. Firstly, we utilized unsupervised UMAP representation on the whole metabolite set and observed a remarkable similarity between young and old ADSC-sEVs treated mice compared to the old control mice (Fig. 5A, Supplementary data 1).

When comparing young and old hearts, we discovered that old mice tend to accumulate a high number of metabolites implicated in several metabolic pathways (62 upregulated and 14 downregulated in Old-PBS mice), such as Acetyl-CoA and related metabolites, GMP, AMP, CMP, or UMP, and short-chain acylcarnitines. On the contrary, young hearts showed an increased concentration of anserine, carnosine, and long-chain acylcarnitines (Fig. 5B). This pattern may indicate a dysregulation of mitochondrial metabolism and fatty acid oxidation, a
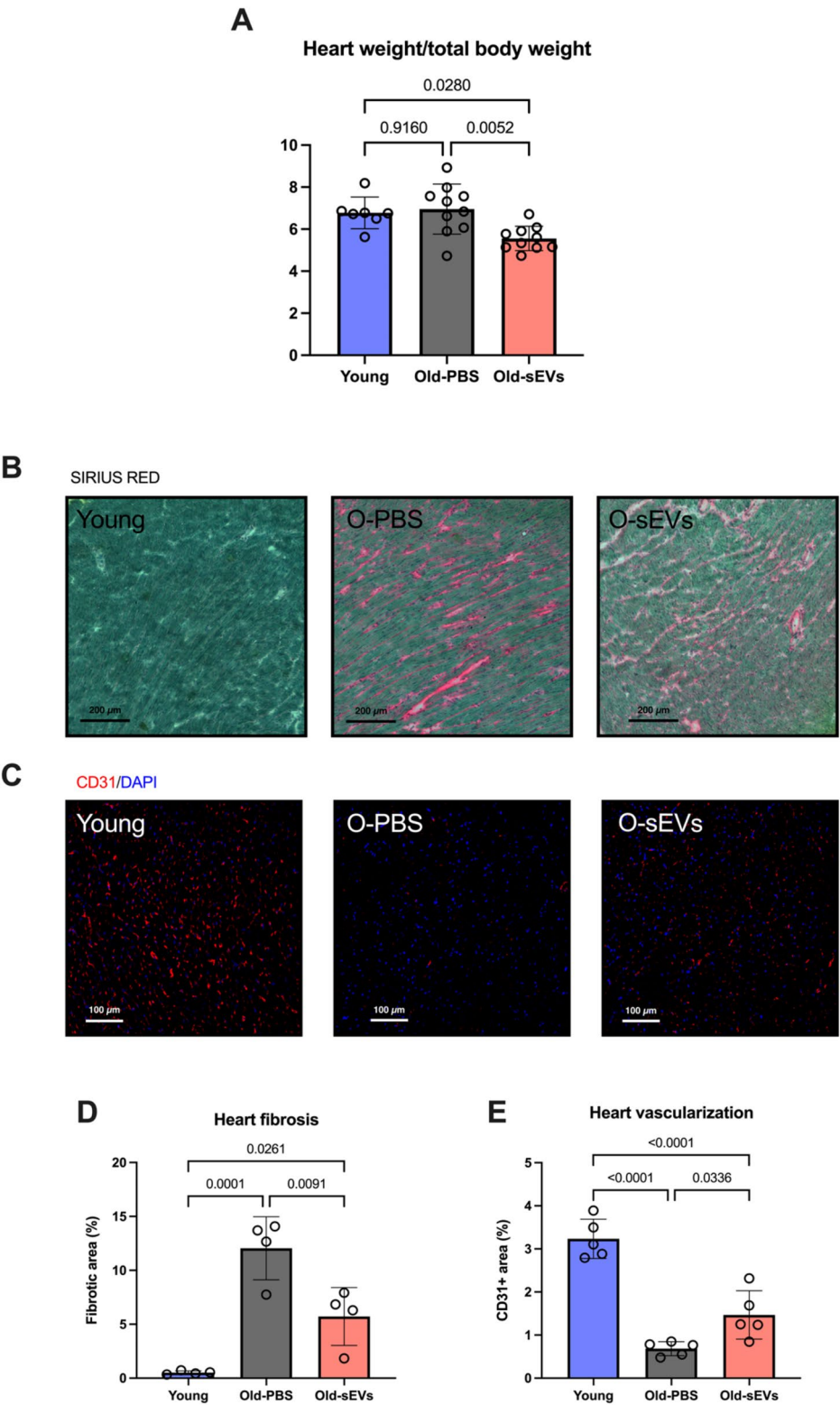
Fig. 3 ADSC-sEVs mitigate structural changes in the mouse heart associated with aging. (**A**) Quantification of the ratio of heart weight divided by TBW. (**B** and **D**) Representative images and quantification of Sirius red staining in heart tissue under light microscopy. (**C** and **E**) Representative images and quantification of CD31 immunofluorescence staining of heart tissue under confocal microscopy. All data are shown as means ± SD. **A**: $n = 7$ for young, 10 for Old-PBS and Old-sEVs. **D**: $n = 4$ per group. **E**: $n = 5$ per group
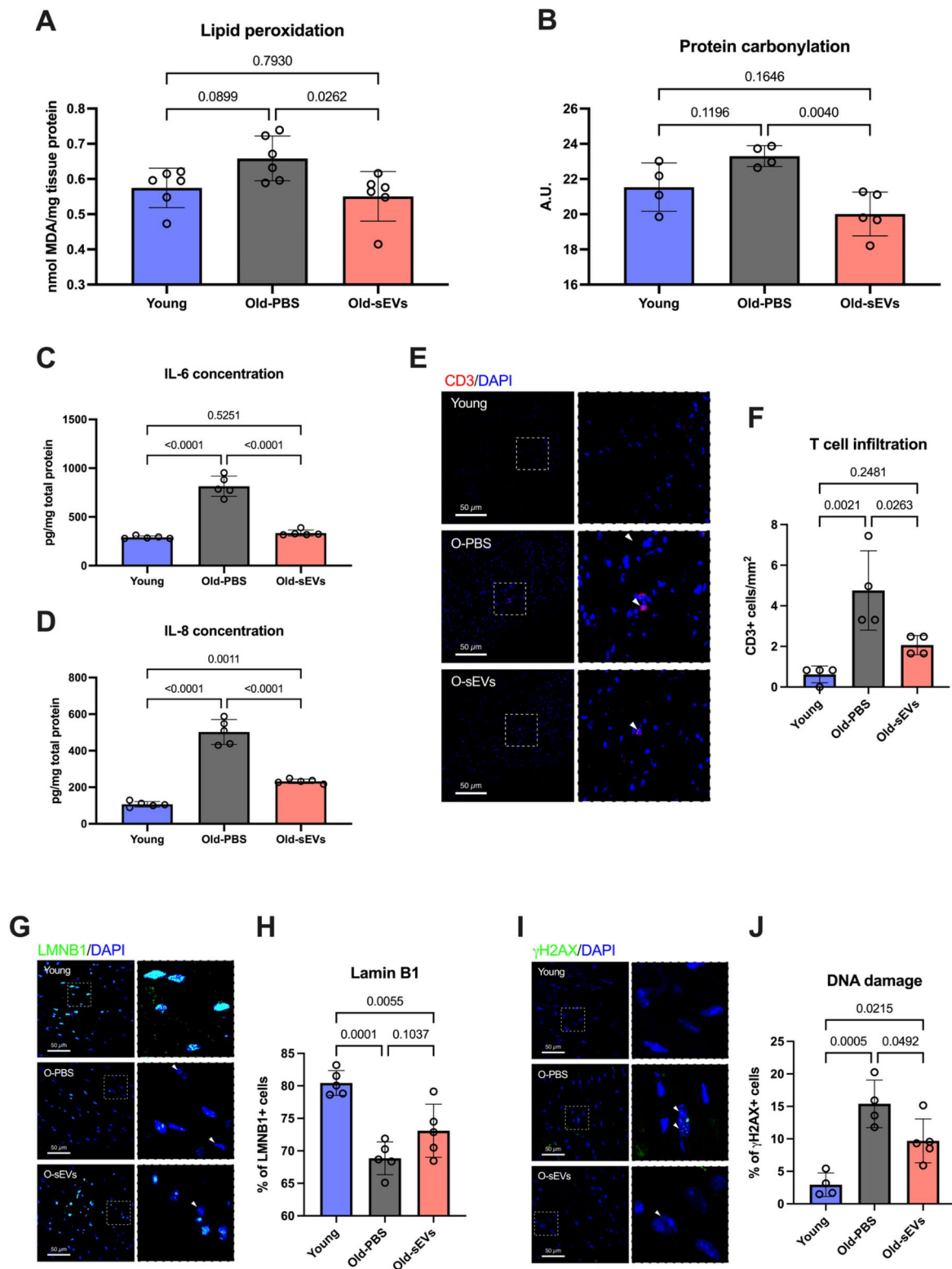
Fig. 4 ADSC-sEVs alleviate cellular and molecular traits associated with aging in the heart of old mice. (**A**) Quantification of lipid peroxidation through determination of MDA levels in heart tissue. (**B**) Quantification of protein carbonylation as a marker of total protein oxidation in the heart tissue. (**C-D**) Quantification of IL-6 and IL-8 levels in heart tissue. (**E-F**) Representative immunofluorescence images and quantification of CD3 + cells in the heart. (**G-H**) Representative immunofluorescence images and quantification of LMNB1 + cells in heart tissue. (**I-J**) Representative immunofluorescence images and quantification of γH2AX + cells in heart tissue. All data are shown as means ± SD. **A**: $n=6$ per group. **B**: $n=4$ for young and Old-PBS, 5 for Old-sEVs. **C-D**: $n=5$ per group. **F**: $n=4$ per group. **H**: $n=5$ per group. **J**: $n=4$ for young and Old-PBS, 5 for Old-sEVs
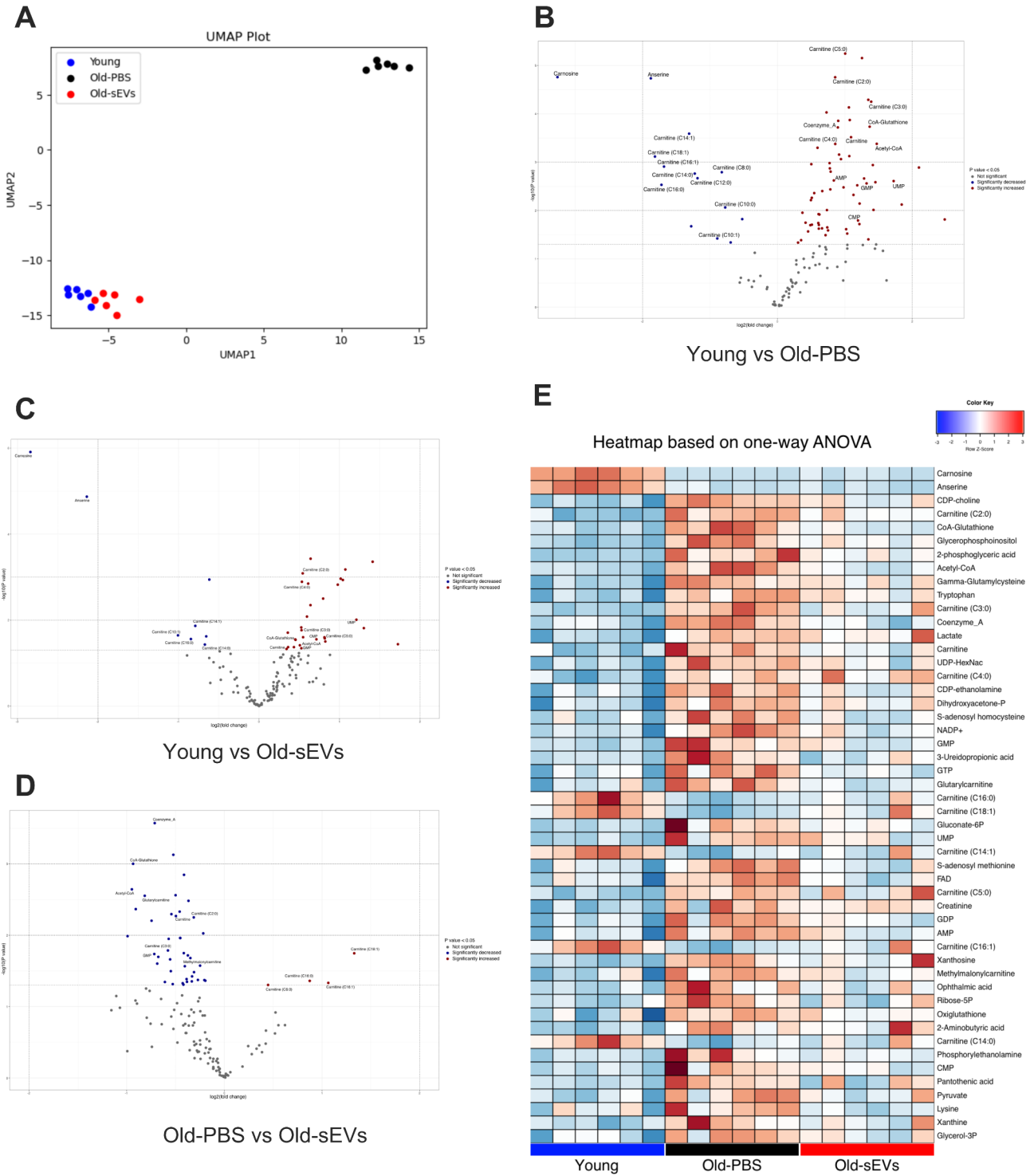
Fig. 5 Metabolomic profiling reveals a youthful signature in ADSC-sEVs treated mice. (**A**) UMAP of the whole metabolite set values from heart tissue of young, Old-PBS and Old-sEVs mice. (**B-D**) Volcano plot showing the different metabolite levels between different comparisons. (**E**) Heatmap of the levels of statistically significant metabolites from ANOVA of the three groups. (**F**) Enrichment ratio (size of the circle) and P values (color of the circle) for the 25 most enriched metabolite sets from a metabolite set enrichment analysis (MSEA) of the significant metabolites. *N* = 6 per group

common finding during aging [32]. Anserine is a natural derivative of carnosine, and both have been implied in cardiac health and aging, as they are essential scavengers of lipid peroxidation products [33–35]. The increased acetyl-CoA levels in old mice could indicate a lower utilization or an increased production; notably, lower cytosolic levels of acetyl-CoA have been linked to increased autophagy and the beneficial effects of caloric restriction during aging [36, 37]. When comparing the heart metabolome of young and old mice treated with ADSC-sEVs, we observed a similar but attenuated pattern, with a tendency to accumulate several metabolites in the old-treated mice but less pronounced (30 upregulated and 8 downregulated in Old-sEVs mice), once again, young mice had higher levels of carnosine, anserine and long-chain acylcarnitines (Fig. 5C). Interestingly, when comparing Old-PBS and Old-sEVs mice, we found an analogous pattern, where Old-sEVs treated mice showed an increased concentration of long-chain acylcarnitines and a downregulation of several metabolites such as acetyl-CoA related (41 downregulated and 4 upregulated in Old-sEVs mice) (Fig. 5D).

To better visualize the changes associated with the treatment in old hearts, we performed a multiple comparison analysis and represented a heatmap of the statistically significant metabolites between the three groups (Fig. 5E). Although it should be the task of future research, old hearts show an increased concentration of short-chain and a reduced concentration of long-chain acylcarnitines, which may indicate that aging influences the heart's preference or ability to utilize different energy substrates. An increase in short-chain acylcarnitines and a decrease in long-chain acylcarnitines might suggest a shift towards using medium or short-chain fatty acids for energy production.

Discussion

The aging process is intricately linked to the decline in tissue function, and the cardiovascular system is one of the most affected. Cardiovascular diseases are the main contributors to late-life mortality in the developed world; therefore, addressing the degenerative changes associated with aging in this system is of great importance. Age-associated alterations of the heart tissues, including fibrosis, valvular degeneration, or cardiomyocyte hypertrophy, are thought to be tightly related to molecular and cellular aspects of aging, such as inflammation, oxidative damage, or cellular senescence [38, 39].

The field of EV research has grown exponentially in the last two decades due to its ability to transport various molecules and factors between cells, making them essential players in intercellular communication. In the area of aging, EVs have shown promise as anti-aging agents. We and other research groups have demonstrated some beneficial effects of EVs from different cell types in specific tissues, such as the kidneys, skeletal muscle, lungs, and the heart. Here, we present a comprehensive study on the effects of ADSC-derived sEVs on the functional, structural, molecular, and cellular parameters that change with aging in the hearts of physiologically aged mice For the functional assessment of heart function, we used echocardiography, as some established changes occur during aging in these animals, which are also common to humans, mainly an increased LV mass and reduced diastolic function, while systolic function is usually not altered [10]. ADSCs-sEVs treatment partially reversed the age-associated increase in LV wall thickness and the altered diastolic function reflected in the E/A wave ratio, in line with previous studies [40]. Additionally, the treadmill physical endurance test revealed beneficial sex-dependent effects of sEVs treatment, emphasizing the need for considering gender-specific responses in anti-aging interventions.

Histological analyses unveiled the impact of ADSC-sEVs on structural changes in the aged heart. Reductions in heart weight related to body weight, fibrotic tissue content, and the enhancement of vascularization collectively suggest a potential protective role of ADSC-sEVs against age-related cardiac remodeling, fibrosis, and impaired vascularization. These results support a growing body of evidence showing the potential of EVs in the modulation of fibrosis and angiogenesis [18, 41]. We also provide insights into the cellular and molecular markers associated with aging in the heart. Notably, treatment with ADSC-sEVs was able to reverse the pattern of increased oxidative and DNA damage, inflammation, and cellular senescence present during aging in the mouse heart. All these processes are firmly linked, as different types of damage to the cellular integrity predispose to the acquisition of the senescent phenotype. Interestingly, cellular senescence has traditionally been viewed as a property of proliferating cells; however, the heart, as a tissue whose primary cells are post-mitotic, also shows characteristics of cellular senescence, a trait termed amitosenescence [42]. The senescent phenotype also contributes to changes in the extracellular environment that lead to the accumulation of pro-inflammatory factors during aging [43]. This SASP, in turn, leads to increased cellular damage and paracrine senescence, a feedback loop thought to contribute substantially to tissue dysfunction during aging and a target of many anti-aging interventions [44–47]. EVs, in part due to their anti-inflammatory properties [48], are believed to counteract this loop in a senomorphic manner, shifting the extracellular environment to a non-senescent phenotype and thus reducing paracrine senescence [4, 49].

Finally, we demonstrated specific changes in a subset of metabolites that are altered in the aged heart and the

influence of ADSC-sEVs on them through metabolomic profiling of heart tissue. These changes include a tendency to accumulate acyl-CoA-related metabolites, possibly because of an inability to use different substrates. Interestingly, we showed that old hearts are prone to accumulate short-chain acylcarnitines and have lower levels of long-chain acylcarnitines. In previous research, acylcarnitine levels in plasma have been associated with cardiovascular events in humans [50]; together with our results, this may indicate a change in fatty acid metabolism in the aged heart. We have also demonstrated that ADSC-sEVs can induce a metabolic shift in the hearts of aged mice, resulting in a metabolomic profile that closely resembles that of younger mice. miRNAs are suggested to play a role mediating the therapeutic effects of EVs, among these, the let-7 family has been extensively studied for their regulatory functions in metabolism as it targets the PI3K/AKT/insulin pathway [51] and it has been shown that this family regulates fatty acid metabolism in cultured cardiomyocytes [52]. Notably, let-7c shows reduced circulating levels in patients with coronary artery disease [53] and the let-7 family is enriched in stem cell-derived EVs [54, 55], suggesting a potential mechanism through which ADSC-sEVs exert their beneficial effects. While these findings are compelling, the specific molecular components within ADSC-sEVs responsible for these changes remain unclear. It is possible that a combination of bioactive molecules, such as miRNAs, lipids, and proteins, contributes to this effect. Further studies are needed to identify these key molecules and to determine whether the observed metabolic changes are a cause or consequence of the broader rejuvenation effects on aging cellular and molecular markers.

Notably, while the observed effects in the heart are significant, we have only analyzed the effects one month after treatment, the transient nature of sEVs impact remains unclear, highlighting the need for follow-up studies to assess long-term benefits and determine whether repeated or sustained interventions are necessary. It is also essential to acknowledge that sEVs were delivered systemically, and their effects are not necessarily confined to cardiac tissue. ADSC-sEVs likely exert a systemic rejuvenation effect by targeting multiple tissues and cellular pathways, collectively contributing to the observed changes. Future investigations should explore the interactions between different tissues in mediating these effects and the underlying mechanisms and translational potential of ADSC-sEVs or other MSC-derived sEVs in combating age-related cardiovascular disease.

Conclusions

In this study, we demonstrate that systemically delivered small extracellular vesicles derived from young adipose-derived stem cells (ADSCs-sEVs) enhance functional parameters related to aging and HFpEF in aged mice. ADSCs-sEVs improve structural and molecular parameters linked to aging in the heart, including fibrosis, vascularization, cellular senescence, inflammation, and oxidative stress. Furthermore, ADSCs-sEVs treatment shifts the heart's metabolome to a younger state. Our findings provide further evidence of the therapeutic potential of EVs in addressing aging and cardiovascular disease, serving as a strategy to mitigate age-related cardiac tissue changes.

Supplementary Information

The online version contains supplementary material available at https://doi.org/10.1186/s13287-025-04255-z.

Supplementary Material 1

Author contributions

Conceptualization: J.S.-R. and C.B. Methodology: J.S.-R., J.H.A., C.M.-B., N.R.-G., M.D. and M.W. Investigation: J.S.-R., J.H.A., C.M.-B., N.R.-G., M.D. and M.W. Visualization: J.S.-R. and C.B. Supervision: G.J and C.B. Writing—original draft: J.S.-R., M.W., and C.B. Writing—review and editing: G.E. and C.B.

Data availability

The datasets generated and/or analyzed during this study are available in the main text or supplementary files, or they can be requested from the corresponding author upon reasonable request. Mass spectrometry data (mzML files) from the metabolomic analysis of heart tissue are publicly available through MetaboLights (https://www.ebi.ac.uk/metabolights/MTBLS12251).

Declarations

Ethics approval and consent to participate

This study was conducted strictly with all applicable national and institutional policies. The protocol received approval from the University of Valencia Animal Ethics Committee following European Union (EU) regulations on animal research (identification number A1508582840889, title: "Efecto de la administración de vesículas extracelulares de células madre de tejido adiposo derivadas de ratones jóvenes en ratones envejecidos/Effect of the administration of extracellular vesicles from adipose-derived stem cells from young mice in old mice", approved on 31-01-2018).

Consent for publication

Not applicable.

Competing interests

None of the authors declare any conflict of interest.

Author details
[1]MiniAging Research Group, Department of Physiology, Faculty of Medicine, University of Valencia, CIBERFES, INCLIVA, Avenida Blasco Ibáñez, 15, Valencia, Spain
[2]Present address: Department of Pathology, Stanford University School of Medicine, Stanford, CA 94305, USA
[3]Department of Anesthesiology and Surgical Trauma Intensive Care, Hospital Clinic Universitari Valencia, University of Valencia, Valencia 46010, Spain
[4]Laboratory Genetic Metabolic Diseases, Amsterdam UMC, Amsterdam Gastroenterology, Endocrinology, and Metabolism, University of Amsterdam, Amsterdam, The Netherlands
[5]Core Facility Metabolomics, Amsterdam UMC, University of Amsterdam, Amsterdam, The Netherlands

References
1. Raposo G, Stoorvogel W. Extracellular vesicles: exosomes, microvesicles, and friends. J Cell Biol. 2013;200(4):373–83.
2. Théry C, Witwer KW, Aikawa E, Alcaraz MJ, Anderson JD, Andriantsitohaina R, Antoniou A, Arab T, Archer F, Atkin-Smith GK, et al. Minimal information for studies of extracellular vesicles 2018 (MISEV2018): a position statement of the international society for extracellular vesicles and update of the MISEV2014 guidelines. J Extracell Vesicles. 2018;7(1):1535750.
3. Yu G, Wu X, Kilroy G, Halvorsen YD, Gimble JM, Floyd ZE. Isolation of murine adipose-derived stem cells. Methods Mol Biol. 2011;702:29–36.
4. Sanz-Ros J, Romero-García N, Mas-Bargues C, Monleón D, Gordevicius J, Brooke RT, Dromant M, Díaz A, Derevyanko A, Guío-Carrión A, et al. Small extracellular vesicles from young adipose-derived stem cells prevent frailty, improve health span, and decrease epigenetic age in old mice. Sci Adv. 2022;8(42):eabq2226.
5. Schomakers BV, Hermans J, Jaspers YRJ, Salomons G, Vaz FM, van Weeghel M, Houtkooper RH. Polar metabolomics in human muscle biopsies using a liquid-liquid extraction and full-scan LC-MS. STAR Protoc. 2022;3(2):101302.
6. Molenaars M, Schomakers BV, Elfrink HL, Gao AW, Vervaart MAT, Pras-Raves ML, Luyf AC, Smith RL, Sterken MG, Kammenga JE et al. Metabolomics and lipidomics in Caenorhabditis elegans using a single-sample Preparation. Dis Model Mech 2021, 14(4).
7. Rohart F, Gautier B, Singh A, Lê Cao KA. MixOmics: an R package for 'omics feature selection and multiple data integration. PLoS Comput Biol. 2017;13(11):e1005752.
8. Thévenot EA, Roux A, Xu Y, Ezan E, Junot C. Analysis of the human adult urinary metabolome variations with age, body mass index, and gender by implementing a comprehensive workflow for univariate and OPLS statistical analyses. J Proteome Res. 2015;14(8):3322–35.
9. Kang M, Jordan V, Blenkiron C, Chamley LW. Biodistribution of extracellular vesicles following administration into animals: A systematic review. J Extracell Vesicles. 2021;10(8):e12085.
10. Zhang TY, Zhao BJ, Wang T, Wang J. Effect of aging and sex on cardiovascular structure and function in wildtype mice assessed with echocardiography. Sci Rep. 2021;11(1):22800.
11. De Moudt S, Hendrickx JO, Neutel C, De Munck D, Leloup A, De Meyer GRY, Martinet W, Fransen P. Progressive aortic stiffness in aging C57Bl/6 mice displays altered contractile behaviour and extracellular matrix changes. Commun Biol. 2022;5(1):605.
12. Paulus WJ, Tschöpe C. A novel paradigm for heart failure with preserved ejection fraction: comorbidities drive myocardial dysfunction and remodeling through coronary microvascular endothelial inflammation. J Am Coll Cardiol. 2013;62(4):263–71.
13. Kane AE, Bisset ES, Heinze-Milne S, Keller KM, Grandy SA, Howlett SE. Maladaptive changes associated with cardiac aging are Sex-Specific and graded by frailty and inflammation in C57BL/6 mice. J Gerontol Biol Sci Med Sci. 2021;76(2):233–43.
14. Suchacki KJ, Thomas BJ, Ikushima YM, Chen KC, Fyfe C, Tavares AAS, Sulston RJ, Lovdel A, Woodward HJ, Han X et al. The effects of caloric restriction on adipose tissue and metabolic health are sex- and age-dependent. Elife 2023, 12.
15. Miller RA, Harrison DE, Astle CM, Fernandez E, Flurkey K, Han M, Javors MA, Li X, Nadon NL, Nelson JF, et al. Rapamycin-mediated lifespan increase in mice is dose and sex dependent and metabolically distinct from dietary restriction. Aging Cell. 2014;13(3):468–77.
16. Hemanthakumar KA, Fang S, Anisimov A, Mäyränpää MI, Mervaala E, Kivelä R. Cardiovascular disease risk factors induce mesenchymal features and senescence in mouse cardiac endothelial cells. Elife 2021, 10.
17. Sangaralingham SJ, Huntley BK, Martin FL, McKie PM, Bellavia D, Ichiki T, Harders GE, Chen HH, Burnett JC. The aging heart, myocardial fibrosis, and its relationship to Circulating C-type natriuretic peptide. Hypertension. 2011;57(2):201–7.
18. Todorova D, Simoncini S, Lacroix R, Sabatier F, Dignat-George F. Extracellular vesicles in angiogenesis. Circ Res. 2017;120(10):1658–73.
19. Xin H, Li Y, Cui Y, Yang JJ, Zhang ZG, Chopp M. Systemic administration of exosomes released from mesenchymal stromal cells promote functional recovery and neurovascular plasticity after stroke in rats. J Cereb Blood Flow Metab. 2013;33(11):1711–5.
20. Lopez-Otin C, Blasco MA, Partridge L, Serrano M, Kroemer G. Hallmarks of aging: an expanding universe. Cell. 2023;186(2):243–78.
21. Walsh C, Choudhury S, Chen MH. Landscape of somatic mutations in aging human heart muscle cells. Nat Aging. 2022;2(8):686–7.
22. Ayala A, Muñoz MF, Argüelles S. Lipid peroxidation: production, metabolism, and signaling mechanisms of malondialdehyde and 4-hydroxy-2-nonenal. Oxid Med Cell Longev. 2014;2014:360438.
23. Fedorova M, Bollineni RC, Hoffmann R. Protein carbonylation as a major hallmark of oxidative damage: update of analytical strategies. Mass Spectrom Rev. 2014;33(2):79–97.
24. Franceschi C, Bonafe M, Valensin S, Olivieri F, De Luca M, Ottaviani E, De Benedictis G. Inflamm-aging. An evolutionary perspective on Immunosenescence. Ann N Y Acad Sci. 2000;908:244–54.
25. Zhu Y, Tchkonia T, Pirtskhalava T, Gower AC, Ding H, Giorgadze N, Palmer AK, Ikeno Y, Hubbard GB, Lenburg M, et al. The Achilles' heel of senescent cells: from transcriptome to senolytic drugs. Aging Cell. 2015;14(4):644–58.
26. Wang Y, Zhu S, Wei W, Tu Y, Chen C, Song J, Li J, Wang C, Xu Z, Sun S. Interleukin-6 knockout reverses macrophage differentiation imbalance and alleviates cardiac dysfunction in aging mice. Aging. 2020;12(20):20184–97.
27. Zhao L, Cheng G, Jin R, Afzal MR, Samanta A, Xuan YT, Girgis H, Elias HK, Zhu Y, Davani A, et al. Deletion of Interleukin-6 attenuates pressure Overload-Induced left ventricular hypertrophy and dysfunction. Circ Res. 2016;118(12):1918–29.
28. Freund A, Laberge RM, Demaria M, Campisi J. Lamin B1 loss is a senescence-associated biomarker. Mol Biol Cell. 2012;23(11):2066–75.
29. Xie S, Xu SC, Deng W, Tang Q. Metabolic landscape in cardiac aging: insights into molecular biology and therapeutic implications. Signal Transduct Target Ther. 2023;8(1):114.
30. Lesnefsky EJ, Chen Q, Hoppel CL. Mitochondrial metabolism in aging heart. Circ Res. 2016;118(10):1593–611.
31. Sithara T, Drosatos K. Metabolic complications in cardiac aging. Front Physiol. 2021;12:669497.
32. Lopez-Otin C, Blasco MA, Partridge L, Serrano M, Kroemer G. The hallmarks of aging. Cell. 2013;153(6):1194–217.
33. Zhao J, Conklin DJ, Guo Y, Zhang X, Obal D, Guo L, Jagatheesan G, Katragadda K, He L, Yin X, et al. Cardiospecific overexpression of ATPGD1 (Carnosine Synthase) increases histidine dipeptide levels and prevents myocardial ischemia reperfusion injury. J Am Heart Assoc. 2020;9(12):e015222.
34. Zhao J, Posa DK, Kumar V, Hoetker D, Kumar A, Ganesan S, Riggs DW, Bhatnagar A, Wempe MF, Baba SP. Carnosine protects cardiac myocytes against lipid peroxidation products. Amino Acids. 2019;51(1):123–38.
35. Caruso G, Di Pietro L, Cardaci V, Maugeri S, Caraci F. The therapeutic potential of carnosine: focus on cellular and molecular mechanisms. Curr Res Pharmacol Drug Discov. 2023;4:100153.
36. Eisenberg T, Schroeder S, Andryushkova A, Pendl T, Küttner V, Bhukel A, Mariño G, Pietrocola F, Harger A, Zimmermann A, et al. Nucleocytosolic depletion of the energy metabolite acetyl-coenzyme a stimulates autophagy and prolongs lifespan. Cell Metab. 2014;19(3):431–44.
37. Mariño G, Pietrocola F, Eisenberg T, Kong Y, Malik SA, Andryushkova A, Schroeder S, Pendl T, Harger A, Niso-Santano M, et al. Regulation of autophagy by cytosolic acetyl-coenzyme A. Mol Cell. 2014;53(5):710–25.
38. Gevaert AB, Shakeri H, Leloup AJ, Van Hove CE, De Meyer GRY, Vrints CJ, Lemmens K, Van Craenenbroeck EM. Endothelial senescence contributes to heart failure with preserved ejection fraction in an aging mouse model. Circ Heart Fail 2017, 10(6).

39. Liberale L, Badimon L, Montecucco F, Lüscher TF, Libby P, Camici GG. Inflammation, aging, and cardiovascular disease: JACC review topic of the week. J Am Coll Cardiol. 2022;79(8):837–47.

40. Grigorian Shamagian L, Rogers RG, Luther K, Angert D, Echavez A, Liu W, Middleton R, Antes T, Valle J, Fourier M, et al. Rejuvenating effects of young extracellular vesicles in aged rats and in cellular models of human senescence. Sci Rep. 2023;13(1):12240.

41. Lv K, Wang Y, Lou P, Liu S, Zhou P, Yang L, Lu Y, Cheng J, Liu J. Extracellular vesicles as advanced therapeutics for the resolution of organ fibrosis: current progress and future perspectives. Front Immunol. 2022;13:1042983.

42. Anderson R, Lagnado A, Maggiorani D, Walaszczyk A, Dookun E, Chapman J, Birch J, Salmonowicz H, Ogrodnik M, Jurk D et al. Length-independent telomere damage drives post-mitotic cardiomyocyte senescence. EMBO J 2019, 38(5).

43. Tchkonia T, Zhu Y, van Deursen J, Campisi J, Kirkland JL. Cellular senescence and the senescent secretory phenotype: therapeutic opportunities. J Clin Invest. 2013;123(3):966–72.

44. Franceschi C, Campisi J. Chronic inflammation (inflammaging) and its potential contribution to age-associated diseases. J Gerontol Biol Sci Med Sci. 2014;69(Suppl 1):S4–9.

45. Kennedy BK, Berger SL, Brunet A, Campisi J, Cuervo AM, Epel ES, Franceschi C, Lithgow GJ, Morimoto RI, Pessin JE, et al. Geroscience: linking aging to chronic disease. Cell. 2014;159(4):709–13.

46. Chang J, Wang Y, Shao L, Laberge RM, Demaria M, Campisi J, Janakiraman K, Sharpless NE, Ding S, Feng W, et al. Clearance of senescent cells by ABT263 rejuvenates aged hematopoietic stem cells in mice. Nat Med. 2016;22(1):78–83.

47. Baar MP, Brandt RMC, Putavet DA, Klein JDD, Derks KWJ, Bourgeois BRM, Stryeck S, Rijksen Y, van Willigenburg H, Feijtel DA, et al. Targeted apoptosis of senescent cells restores tissue homeostasis in response to chemotoxicity and aging. Cell. 2017;169(1):132–e147116.

48. Ryan ST, Hosseini-Beheshti E, Afrose D, Ding X, Xia B, Grau GE, Little CB, McClements L, Li JJ. Extracellular vesicles from mesenchymal stromal cells for the treatment of Inflammation-Related conditions. Int J Mol Sci 2021, 22(6).

49. Dorronsoro A, Santiago FE, Grassi D, Zhang T, Lai RC, McGowan SJ, Angelini L, Lavasani M, Corbo L, Lu A, et al. Mesenchymal stem cell-derived extracellular vesicles reduce senescence and extend health span in mouse models of aging. Aging Cell. 2021;20(4):e13337.

50. Shah SH, Sun JL, Stevens RD, Bain JR, Muehlbauer MJ, Pieper KS, Haynes C, Hauser ER, Kraus WE, Granger CB, et al. Baseline metabolomic profiles predict cardiovascular events in patients at risk for coronary artery disease. Am Heart J. 2012;163(5):844–e850841.

51. Zhu H, Shyh-Chang N, Segrè AV, Shinoda G, Shah SP, Einhorn WS, Takeuchi A, Engreitz JM, Hagan JP, Kharas MG, et al. The Lin28/let-7 axis regulates glucose metabolism. Cell. 2011;147(1):81–94.

52. Kuppusamy KT, Jones DC, Sperber H, Madan A, Fischer KA, Rodriguez ML, Pabon L, Zhu WZ, Tulloch NL, Yang X, et al. Let-7 family of MicroRNA is required for maturation and adult-like metabolism in stem cell-derived cardiomyocytes. Proc Natl Acad Sci U S A. 2015;112(21):E2785–2794.

53. Faccini J, Ruidavets JB, Cordelier P, Martins F, Maoret JJ, Bongard V, Ferrières J, Roncalli J, Elbaz M, Vindis C. Circulating miR-155, miR-145 and let-7c as diagnostic biomarkers of the coronary artery disease. Sci Rep. 2017;7:42916.

54. Lin D, Chen H, Xiong J, Zhang J, Hu Z, Gao J, Gao B, Zhang S, Chen J, Cao H, et al. Mesenchymal stem cells Exosomal let-7a-5p improve autophagic flux and alleviate liver injury in acute-on-chronic liver failure by promoting nuclear expression of TFEB. Cell Death Dis. 2022;13(10):865.

55. Suzuki H, Yokoi A, Uno K, Yoshida K, Kitagawa M, Asano-Inami E, Matsuo S, Nagao Y, Suzuki K, Nakamura K, et al. Small extracellular vesicles from adipose-derived stem cells suppress cell proliferation by delivering the let-7 family of MicroRNAs in ovarian cancer. Biochem Biophys Res Commun. 2023;680:211–9.

Publisher's note